AMERICAN SOCIETY FOR MICROBIOLOGY | Journal of Bacteriology®

RESEARCH ARTICLE

A Defective Undecaprenyl Pyrophosphate Synthase Induces Growth and Morphological Defects That Are Suppressed by Mutations in the Isoprenoid Pathway of *Escherichia coli*

William J. MacCain,[a] Suresh Kannan,[a] Dannah Z. Jameel,[b] Jerry M. Troutman,[b] Kevin D. Young[a]

[a]Department of Microbiology and Immunology, University of Arkansas for Medical Sciences, Little Rock, Arkansas, USA

[b]Department of Chemistry, University of North Carolina Charlotte, Charlotte, North Carolina, USA

ABSTRACT The peptidoglycan exoskeleton shapes bacteria and protects them against osmotic forces, making its synthesis the target of many current antibiotics. Peptidoglycan precursors are attached to a lipid carrier and flipped from the cytoplasm into the periplasm to be incorporated into the cell wall. In *Escherichia coli*, this carrier is undecaprenyl phosphate (Und-P), which is synthesized as a diphosphate by the enzyme undecaprenyl pyrophosphate synthase (UppS). *E. coli* MG1655 exhibits wild-type morphology at all temperatures, but one of our laboratory strains (CS109) was highly aberrant when grown at 42°C. This strain contained mutations affecting the Und-P synthetic pathway genes *uppS*, *ispH*, and *idi*. Normal morphology was restored by overexpressing *uppS* or by replacing the mutant (*uppS31*) with the wild-type allele. Importantly, moving *uppS31* into MG1655 was lethal even at 30°C, indicating that the altered enzyme was highly deleterious, but growth was restored by adding the CS109 versions of *ispH* and *idi*. Purified UppS^{W31R} was enzymatically defective at all temperatures, suggesting that it could not supply enough Und-P during rapid growth unless suppressor mutations were present. We conclude that cell wall synthesis is profoundly sensitive to changes in the pool of polyisoprenoids and that isoprenoid homeostasis exerts a particularly strong evolutionary pressure.

IMPORTANCE Bacterial morphology is determined primarily by the overall structure of the semirigid macromolecule peptidoglycan. Not only does peptidoglycan contribute to cell shape, but it also protects cells against lysis caused by excess osmotic pressure. Because it is critical for bacterial survival, it is no surprise that many antibiotics target peptidoglycan biosynthesis. However, important gaps remain in our understanding about how this process is affected by peptidoglycan precursor availability. Here, we report that a mutation altering the enzyme that synthesizes Und-P prevents cells from growing at high temperatures and that compensatory mutations in enzymes functioning upstream of *uppS* can reverse this phenotype. The results highlight the importance of Und-P metabolism for maintaining normal cell wall synthesis and shape.

KEYWORDS UppS, isoprenoid, undecaprenyl phosphate, peptidoglycan, morphology, Und-P, isoprenoids

Isoprenoids, also referred to as terpenoids or terpenes (1, 2), are one of nature's most chemically diverse families and are produced by organisms in all three biological kingdoms (1–4). Some of these polyisoprenyl lipid carrier compounds are required for synthesizing peptidoglycan (PG) and membranes, as well as for synthesizing the ubiquinones that enable aerobic respiration (5, 6). In addition, the newly invigorated field of metabolic engineering is creating or manipulating such isoprenoids for producing new pharmaceuticals, flavorings, vitamins, and agrochemicals at low cost and in

Received 27 April 2018 **Accepted** 5 July 2018

Accepted manuscript posted online 9 July 2018

Citation MacCain WJ, Kannan S, Jameel DZ, Troutman JM, Young KD. 2018. A defective undecaprenyl pyrophosphate synthase induces growth and morphological defects that are suppressed by mutations in the isoprenoid pathway of *Escherichia coli*. J Bacteriol 200:e00255-18. https://doi.org/10.1128/JB.00255-18.

Editor Yves V. Brun, Indiana University Bloomington

Address correspondence to Kevin D. Young, kdyoung@uams.edu.

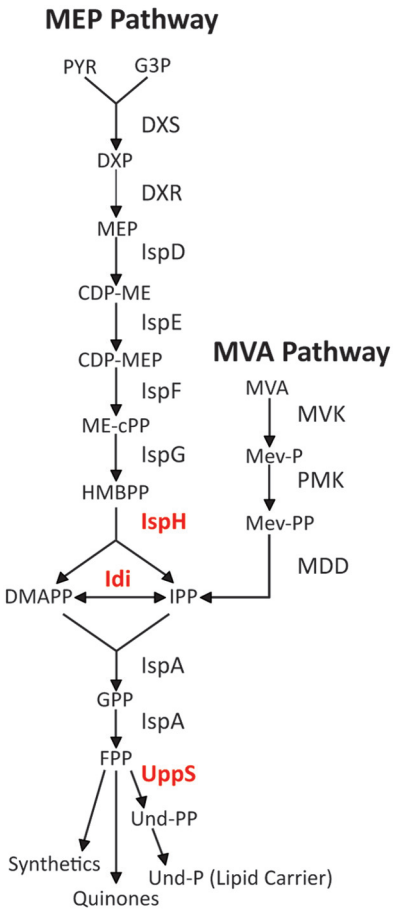

FIG 1 The methylerythritol phosphate (MEP) and mevalonate phosphate (MVA) pathways. Enzyme designations are associated with each step in the pathways (arrows). The three enzymes in red are discussed further in the text: IspH, diphosphate reductase; Idi, isopentenyl diphosphate isomerase; and UppS, undecaprenyl diphosphate synthase. PYR, pyruvate; G3P, glyceraldehyde 3-phosphate; DXP, 1-deoxy-D-xylulose 5-phosphate; MEP, 2*C*-methyl-D-erythritol 4-phosphate; CDP-ME, 4-diphosphocytidyl-2*C*-methyl-D-erythritol, CDP-MEP, CDP-ME-2-phosphate; ME-cPP, 2*C*-methyl-D-erythritol 2,4-cyclodiphosphate; HMBPP, 1-hydroxyl-2-methyl-2-(E)-butenyl 4-diphosphate; IPP, isopentenyl diphosphate; DMAPP, dimethylallyl diphosphate; GPP, geranyl diphosphate; FPP, farnesyl diphosphate; Und-PP, undecaprenyl pyrophosphate; MVA, mevalonate; Mev-P, mevalonate 5-phosphate; Mev-PP, mevalonate pyrophosphate; MVK, mevalonate kinase; PMK, phosphomevalonate kinase; MDD, mevalonate pyrophosphate decarboxylase.

large amounts (2, 7–9). The ubiquity, essentiality, and utility of the isoprenoids demonstrate how important it is to understand more fully the enzymes and pathways that make and modify them.

All isoprenoids are made from two basic five-carbon precursor units, isopentenyl diphosphate (IPP) and its isomer, dimethylallyl diphosphate (DMAPP) (3). The extreme variety of the eventual products arises by combining different numbers of these two substrates in varied ways (7, 9). In *Escherichia coli* and most other bacteria, IPP and DMAPP are synthesized via the methylerythritol phosphate (MEP) pathway, while eukaryotes, most archaea, and certain Gram-positive cocci (*Staphylococcus* and *Enterococcus* spp.) make the same compounds via the mevalonate (MEV or MVA) pathway (2, 9). In *E. coli*, the first committed step in the MEP pathway is catalyzed by 1-deoxy-D-xylulose 5-phosphate (DXP) synthase (DXS), which condenses pyruvate and glyceraldehyde 3-phosphate to synthesize DXP (Fig. 1) (10). After several intermediate reactions (Fig. 1), IspH (4-hydroxy-3-methyl-butenyl-1-diphosphate [HMBPP] reductase) produces both IPP and DMAPP, after which the ratio of these compounds is adjusted by the isomerase Idi (11), and IspA combines two IPP with one DMAPP to generate farnesyl diphosphate (FPP or C_{15}-PP) (Fig. 1). At this point, the pathway branches, with FPP

being used as the initial substrate for synthesizing several products, including undecaprenyl phosphate (Und-P), ubiquinone, and other isoprenoids (Fig. 1) (12).

In all cells, the primary lipid carrier molecule is a membrane-associated polyprenol (5, 13). This compound constitutes a biochemical branch point that may become a bottleneck because the carrier serves multiple pathways that transfer sugars and polysaccharides across the cytoplasmic membrane (13). In Gram-negative bacteria, such as *E. coli*, these products end up in the periplasm or on the exterior of the outer membrane, while in Gram-positive bacteria and in eukaryotic cells, analogous products are shuttled to the external milieu or across the endoplasmic reticulum (14, 15). In bacteria, either Und-P or decaprenyl phosphate (Dec-P) performs this duty during the synthesis of several polymeric glycans, including cell wall peptidoglycan (16, 17), wall teichoic acids (18), enterobacterial common antigen (19), O antigen (20), capsules (21), and other polysaccharides (22–26). In *E. coli*, undecaprenyl pyrophosphate synthase (UppS) adds eight units of IPP to FPP to yield undecaprenyl pyrophosphate (Und-PP), a 55-carbon isoprenoid also known as bactoprenol-PP or C_{55}-PP, which is then dephosphorylated to yield Und-P (Fig. 1) (27). A suite of glycosyltransferases links one or more sugar residues to Und-P, and these intermediates are translocated across the cytoplasmic membrane where they may be modified before being transferred onto recipient polysaccharides or proteins (28–32). This last reaction releases free Und-PP, which is returned to the cytoplasm either before or after being dephosphorylated to Und-P, and this recycled Und-P repeats the carbohydrate transfer process for the same or a different pathway (33).

Given their fundamental importance, it is not surprising that mutations in isoprenoid pathways can affect bacterial growth, but it is intriguing that some of these mutations also alter cell shape (34–39). The usual explanation for either phenotype is that interfering with isoprenoid synthesis alters the rate of production of Und-P, which in turn may affect cell wall synthesis (37, 38, 40, 41). In a similar vein, sequestering Und-P in unusable intermediates also makes it less available for PG synthesis, leading to assorted defects in growth and cell shape (42–44). Nonetheless, what remains unclear is how much Und-P is required for optimal PG synthesis and how the final concentration of Und-P is affected by altered levels of IPP-related substrates.

Here, we find that a laboratory strain of *E. coli*, CS109, is highly misshapen when grown at 42°C, unlike other common strains that produce cells with normal rod shapes at this temperature. In a comparison of the genome of CS109 with that of the canonical strain MG1655, we determined that this phenotype is influenced by three mutations which affect isoprenoid synthesis. In particular, *E. coli* CS109 contains a missense mutation in *uppS* (*uppS31*, which encodes $UppS^{W31R}$). When present by itself, this mutation is extremely deleterious to the growth and morphology of *E. coli* MG1655, even at temperatures as low as 30°C. The other two mutations, in *ispH* or upstream of *idi*, are not themselves injurious but instead relieve the effects associated with *uppS31*, suggesting that these arose as secondary suppressor mutations. This is the first reported phenotype associated with the loss or mutation of *idi* in organisms that use the MEP pathway. Finally, *in vitro* assays with purified $UppS^{W31R}$ indicate that this variant does not synthesize isoprenoids as efficiently as wild-type UppS, regardless of temperature. Overall, the results indicate that bacterial shape is highly sensitive to changes in the availability of the lipid carrier Und-P and that altering individual enzymes in the Und-P synthetic pathway can substantially reverse deleterious mutations in *uppS*.

RESULTS

***E. coli* CS109 exhibits temperature-sensitive cell shape defects.** *E. coli* grows well over a range of temperatures to about 50°C and produces uniformly rod-shaped cells under these conditions, as illustrated by the growth of *E. coli* MG1655 (Fig. 2A and C). Unexpectedly, however, one of our laboratory strains, *E. coli* CS109, grew normally at 30°C (Fig. 2A) but at 42°C produced cells that were swollen and longer (Fig. 2C). At 30°C, these two strains had the same mean cell size (Fig. 2B), but CS109 was ~3.4-fold larger

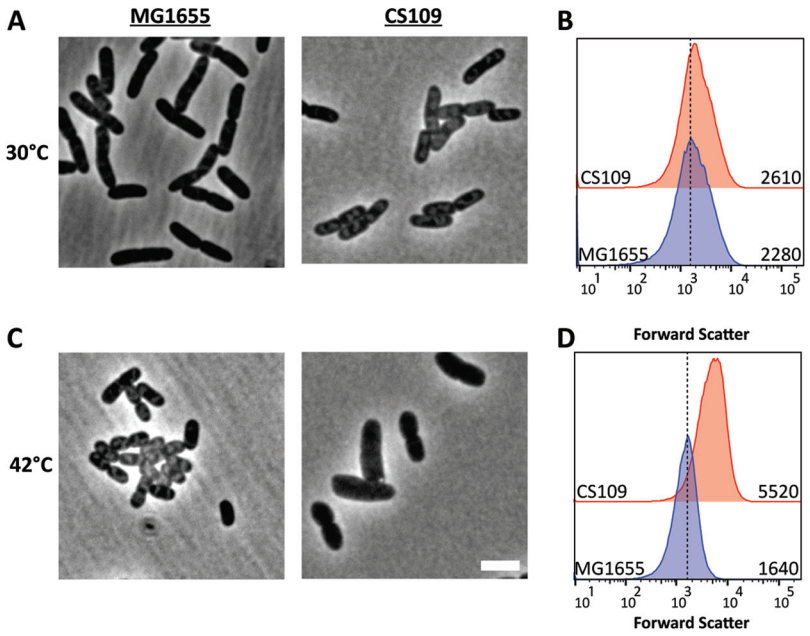

FIG 2 Cells expressing *uppS31* are misshapen at 42°C. (A and C) Cells were grown in LB to an OD_{600} of 0.5 to 0.6 at 30°C (A) and 42°C (C) and photographed by phase-contrast microscopy. The scale bar represents 3 μm. (B and D) Flow cytometry of cells at 30°C (B) and 42°C (D). Shown are histograms of the forward-scatter area of 100,000 live cells of either MG1655 or CS109, as shown in panels A and C. The mean of the forward scatter area is reported in arbitrary units (AU) to the right of each curve. The dashed line represents the mean forward-scatter area of MG1655.

than MG1655 when grown at 42°C (Fig. 2C and D). We previously observed that these two strains differed in other traits, such as motility, spheroplast recovery, and cell spiraling. However, this temperature-sensitive (ts) defect appeared to be unique, so we investigated its cause in more detail, because changes in cell shape often herald problems with cell wall synthesis or cell division (45).

Growth and cell shape are altered by mutations affecting synthesis of Und-P and isoprenoids. By sequencing the genomes of *E. coli* CS109 and MG1655, we found that the two strains differed in a number of ways, including several base pair changes and insertion sequence (IS) insertions (Table 1). With respect to the current work, three differences stood out, i.e., compared to wild-type MG1655, CS109 carried missense versions of *uppS* and *ispH*, as well as an IS*1* insertion 20 bp upstream of *idi* (Table 1). Each of these three gene products helps synthesize Und-P (Fig. 1), the lipid carrier for PG synthesis, suggesting that one or more of these mutations may have affected the synthesis or availability of Und-P as well as cell shape.

TABLE 1 Genomic differences in *E. coli* CS109 and *E. coli* MG1655

Gene	Mutation (amino acid change)	Protein or relevant feature
uppS[a]	T to C (W31R)	Undecaprenyl diphosphate synthase
ispH[a]	T to G (S269A)	1-Hydroxy-2-methyl-2-(*E*)-butenyl-4-diphosphate reductase
rpoS	C to T (Q33Amber)	Sigma S factor
acnA	A to G (S522G)	Aconitase
intQ	T to C (F261L)	Integrase
ygeN	C to A (V195F)	Pseudogene
IGR[b]	T to G	Between *leuX* and *intB′*
idi[a]	IS*1*[c]	Isopentenyl diphosphate isomerase
ydcJ	IS*2*[c]	Unknown function

[a]Genes involved in the methylerithritol phosphate (MEP) pathway for Und-P synthesis.
[b]IGR, intergenic region.
[c]Insertion elements.

CS109 had a T-to-C missense mutation in *uppS* (*uppS31*), the gene encoding undecaprenyl pyrophosphate synthase, thus producing a tryptophan-to-arginine substitution at amino acid 31 (Table 1). To determine if this mutation affected cell shape, we overexpressed cloned versions of *uppS31* or wild-type *uppS*$^+$ in CS109. In cells grown at 42°C, overexpressing *uppS*$^+$ rescued cell shape completely (Fig. 3A) and decreased cell size relative to that observed for CS109 grown at 30°C (compare Fig. 3B to 2B, 2,550 arbitrary units [AU] and 2,610 AU, respectively). Overexpressing *uppS31* partially restored cell shape (Fig. 3A) and reduced cell size substantially compared to the empty vector (Fig. 3B). Thus, UppS^{W31R} was less effective at complementing the shape defect of CS109. We further clarified the importance of *uppS* by moving the wild-type gene onto the chromosome of CS109, replacing the *uppS31* allele with wild-type *uppS* from MG1655 (Fig. 4C and D). At 42°C, CS109 *uppS31* cells were highly misshapen (Fig. 4C) and enlarged (Fig. 4D), but CS109 *uppS*$^+$ cells exhibited normal morphology (Fig. 4C) and cell size (Fig. 4D). At this higher temperature, CS109 *uppS31* cells were ~30% longer and ~44% wider than were CS109 *uppS*$^+$ cells (Table 2), indicating that UppS^{W31R} was responsible for the morphological effects. To confirm this, we moved the *uppS31* allele onto the chromosome of MG1655, replacing the wild-type gene. Surprisingly, MG1655 *uppS31* could not grow in liquid LB medium, even at 30°C (Fig. 4A). In short, the wild-type version UppS reversed the morphological effects in CS109, while UppS^{W31R} was sufficient to impart a dramatic temperature-dependent effect in MG1655. These results indicate that the state of *uppS* is a primary determinant of cell growth and morphology.

Because CS109 grew normally at 30°C, it was surprising that *uppS31* would be so deleterious to the growth of MG1655 at this same temperature. However, two other mutations in CS109 affect the isoprenoid pathway upstream of UppS, *ispH269*, a missense mutant, and an IS*1* insertion sequence 20 bp upstream of the start codon of *idi*, which could alter the expression of this gene product (Table 1). Reasoning that these additional mutations might suppress the effects of *uppS31*, we examined the growth and shape of strains containing different combinations of *uppS* and *ispH* alleles. When the wild-type *uppS*$^+$ gene was present, both CS109 and MG1655 cells exhibited normal rod shapes at 42°C, regardless of whether the wild-type *ispH*$^+$ or *ispH269* allele was present (Fig. 4C to F, and not shown). This confirmed that the state of UppS played the dominant phenotypic role and that the IspH^{S269A} variant did not by itself alter cellular morphology. As for cells containing *uppS31* and incubated at 42°C, CS109 *uppS31* cells containing the wild-type *ispH*$^+$ gene were aberrantly shaped, as were CS109 *uppS31 ispH269* cells (the parental genotype) (Fig. 4C). Flow cytometry indicated that *uppS31 ispH*$^+$ cells (Fig. 4D, 7,160 AU) were about 40% larger than were *uppS31 ispH269* cells (Fig. 4D, 5,120 AU), indicating that IspH^{S269A} partially suppressed the morphological defects associated with UppS^{W31R}. MG1655 *uppS31 ispH*$^+$ cells failed to grow at 42°C, but combining the *ispH269* allele with *uppS31* rescued cell growth at this temperature (Fig. 4E). However, MG1655 *uppS31 ispH269* cells exhibited gross morphological defects (Fig. 4E), as confirmed by the greatly increased light scatter of cells examined by flow cytometry (Fig. 4F). Thus, in MG1655, the *ispH269* mutation suppressed the lethality of *uppS31*, though cell shape did not return to normal at 42°C.

The second potential suppressor mutation was an IS*1* element 20 bp upstream of the start codon of *idi*. Moving *idi* with no upstream IS into CS109 had no effect on the morphology of cells grown at 42°C (Table 3, strain WJM34, and data not shown). In addition, deleting *idi* from CS109 produced cells that were morphologically indistinguishable from cells harboring the IS*1* element upstream of an intact *idi* gene (Table 3, strain WJM8 and not shown). Deleting *idi* or introducing the IS*1* element also had no effect on the shape of MG1655 (Table 3, strains SKMG126 and SKMG124, and data not shown). However, deleting *idi* or introducing the IS*1-idi* construct did restore growth to MG1655 *uppS31* cells at 30°C but not 42°C (Table 3, strains WJM11 and WJM32). Thus, although Idi does not affect cell shape by itself, removing *idi* partially suppresses the effects of *uppS31* by an as-yet-unknown mechanism. To our knowledge, this is the first phenotype associated with the mutation or removal of Idi.

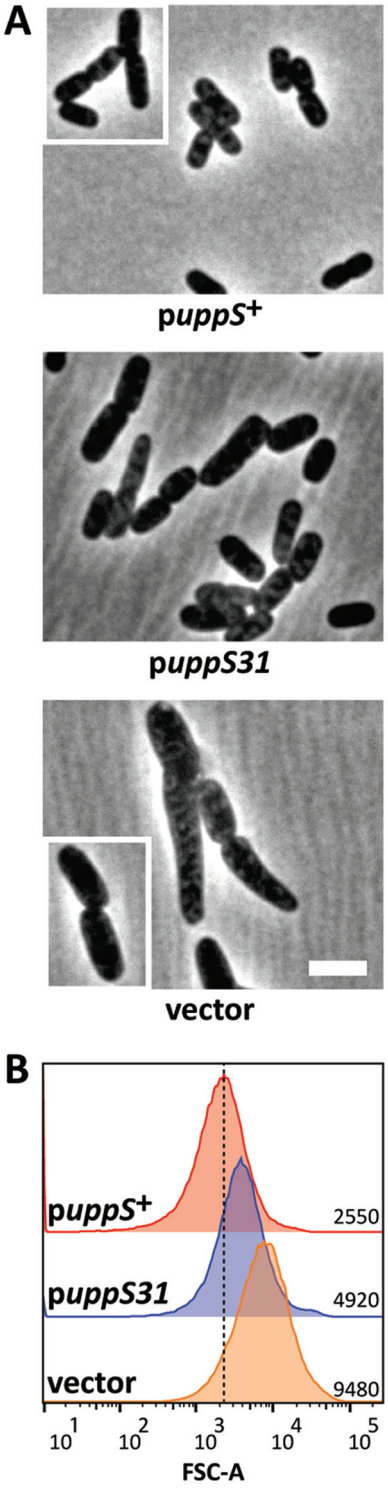

FIG 3 Overexpressing *uppS* restores cell shape to *E. coli* CS109 at 42°C. (A) CS109 harboring plasmids carrying the indicated genes were grown at 42°C in LB plus 25 μM isopropyl-thio-β-D-galactopyranoside (IPTG) to an OD_{600} of 0.5 to 0.6 and photographed by phase-contrast microscopy. The scale bar represents 3 μm. (B) Histograms of the forward-scatter (FSC) area of 100,000 live cells shown in panel A. The mean of the forward-scatter area is reported in arbitrary units (AU) to the right of each curve, and the vertical dashed line represents the mean forward scatter of CS109 alone. p*uppS*$^+$, pMAJ9; p*uppS31*, pUppS; vector, pDSW204.

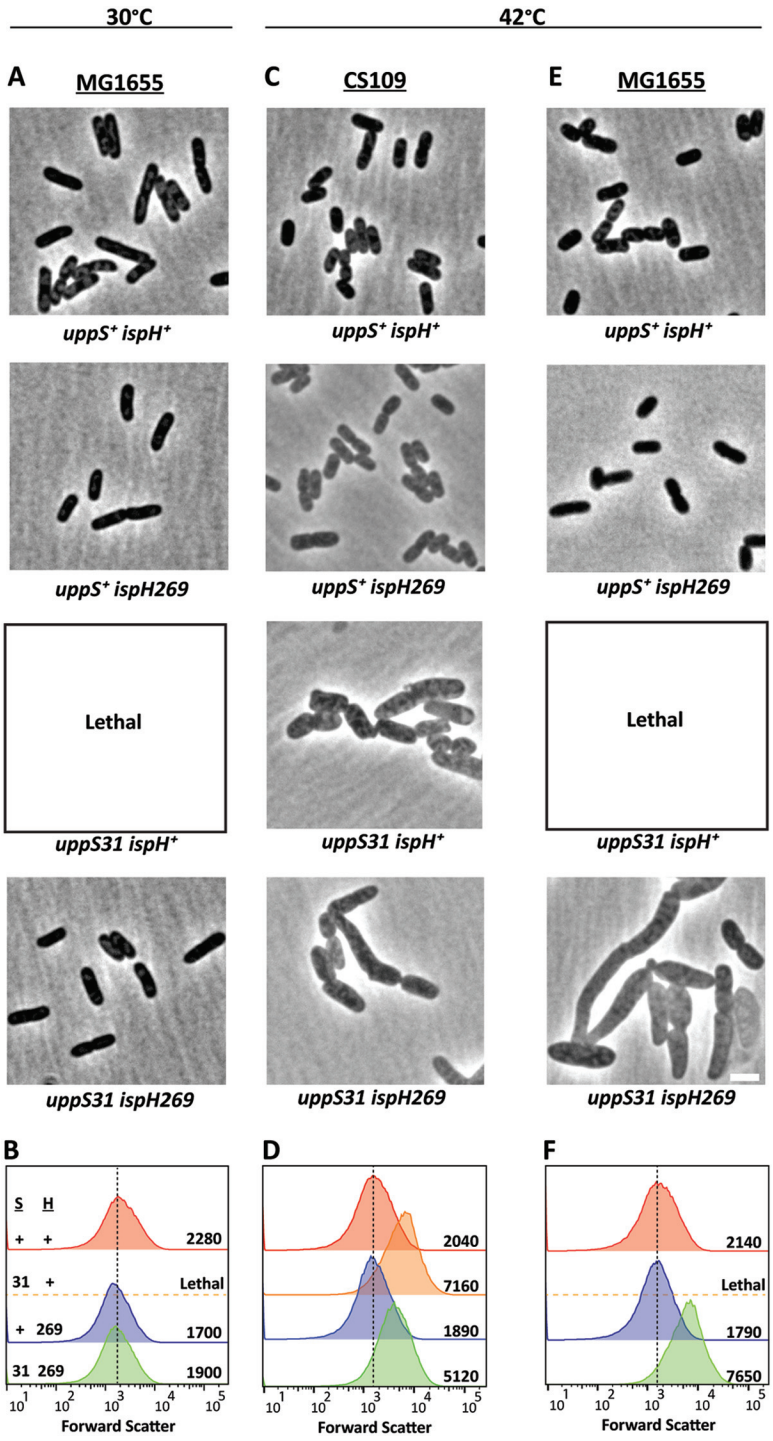

FIG 4 Correcting the *uppS31* missense mutation restores cell shape at 42°C. (A, C, and E) Phase-contrast micrographs of MG1655 (A and E) or CS109 (C) cells carrying wild-type genes (*uppS*$^+$ and *ispH*$^+$) or mutations (*uppS31* and *ispH269*), as noted. MG1655 cells containing *uppS31* combined with wild-type *ispH* did not grow when subcultured in liquid medium (Lethal). Cells were grown in LB at 30°C or 42°C, as noted, to an OD_{600} of 0.5 to 0.6 and were photographed by phase-contrast microscopy. The scale bar represents 3 μm. (B, D, and F) Histograms of the forward scatter of 100,000 live cells as shown in panels A, C, and E. The mean of the forward scatter is reported in arbitrary units to the right of each curve, and the vertical dashed line represents the mean forward scatter of the *uppS*$^+$ *ispH*$^+$ mutant strain for each group. (C and D) Strains CS109 (*uppS31 ispH269*) (green curve), SKCS156 (*uppS*$^+$ *ispH269*) (blue curve), SKCS183 (*uppS31 ispH*$^+$) (orange curve), and SKCS195 (*uppS*$^+$ *ispH*$^+$) (red curve) all with IS-*idi*. (A, B, E, and F) Strains MG1655 (*uppS*$^+$ *ispH*$^+$) (red curve), SKCS173 (*uppS31 ispH*$^+$) (orange curve), SKMG143 (*uppS*$^+$ *ispH269*) (blue curve), and SKMG197 (*uppS31 ispH269*) (green curve) all with no IS upstream of *idi*. S, UppS; H, IspH; +, wild type; 31, UppS^{W31R}; 269, IspH^{S269A}.

TABLE 2 Size of *E. coli* cells containing *uppS*$^+$ or *uppS31*

Strain	Temp (°C)	No. of cells	Cell size (mean ± SD) (μm)	
			Length	Width
MG1655 *uppS*$^+$	30	197	3.37 ± 0.9	1.29 ± 0.1
	42	243	2.81 ± 0.7	1.42 ± 0.1
CS109 *uppS*$^+$	30	166	3.67 ± 0.8	1.36 ± 0.1
	42	311	2.83 ± 0.6	1.30 ± 0.1
CS109 *uppS31*	30	209	3.49 ± 0.9	1.33 ± 0.1
	42	239	3.69 ± 1.2	1.88 ± 0.2

Finally, to determine how much the *ispH* and *idi* alleles each contributed to the suppression of *uppS31*, we compared how well MG1655 *uppS31* strains with different allele combinations grew at temperatures ranging from 30°C to 46°C (Fig. 5). As noted above, MG1655 *uppS31* does not grow at temperatures of 30°C or higher, meaning that growth in this strain will measure the relative abilities of *ispH* and *idi* to suppress the lethality of *uppS31*. In a MG1655 *uppS31 idi*$^+$ background, adding *ispH269* restored robust growth at 30, 37, and 42°C (Fig. 5A). At 44°C, the cells grew well but plateaued at a lower optical density at stationary phase (Fig. 5A). At 45°C and 46°C, the cells grew for 1.0 to 1.5 h, but then the two cultures lysed at approximately the same time (Fig. 5A). Thus, *ispH269* suppresses *uppS31*, but the effect disappears at a sharp temperature cutoff. In contrast, in a *uppS31 ispH*$^+$ background, adding the IS-*idi* construct allowed the cells to grow at a moderate rate at 30 and 37°C, but the cells did not grow at all at 42°C and above (Fig. 5B). Cells from which *idi* was deleted behaved the same way as did those carrying IS-*idi* (not shown), suggesting that in each case suppression was caused by a lack of Idi. Combining both suppressors in MG1655 *uppS31 ispH269* IS-*idi* produced

TABLE 3 Growth and morphology of mutant combinations

Wild type or mutant strain	WT or mutation[a]			Growth at[b]:		Shape at[c]:	
	UppS	IspH	Idi	30°C	42°C	30°C	42°C
MG1655 background							
MG1655	WT	WT	WT	+	+	+	+
SKMG173	31	WT	WT	−	ND	−	ND
SKMG198	31	269	WT	+	+	+	−
WJM11	31	WT	Δ	+	−	−	−
WJM32	31	WT	IS	+	−	−	−
SKMG143	WT	269	WT	+	+	+	+
WJM25	WT	269	Δ	+	+	+	+
WJM30	WT	269	IS	+	+	+	+
SKMG124	WT	WT	Δ	+	+	+	+
SKMG126	WT	WT	IS	+	+	+	+
WJM12	31	269	Δ	+	+	+	−
WJM33	31	269	IS	+	+	+	−
CS109 background							
WJM27	WT	WT	WT	+	+	+	+
WJM31	31	WT	WT	+	+	+	−
WJM34	31	269	WT	+	+	+	−
WJM26	31	WT	Δ	+	+	+	−
SKCS183	31	WT	IS	+	+	+	−
WJM16	WT	269	WT	+	+	+	+
WJM17	WT	269	Δ	+	+	+	+
SKCS156	WT	269	IS	+	+	+	+
WJM29	WT	WT	Δ	+	+	+	+
SKCS195	WT	WT	IS	+	+	+	+
WJM8	31	269	Δ	+	+	+	−
CS109	31	269	IS	+	+	+	−

[a]WT, wild type; 31, UppS^{W31R}; 269, IspH^{S269A}; IS, IS-idi; Δ, Δ*idi*.
[b]+, cells grew; −, cells did not grow; ND, not determined.
[c]+, wild-type cell shape; −, aberrant cell shape.

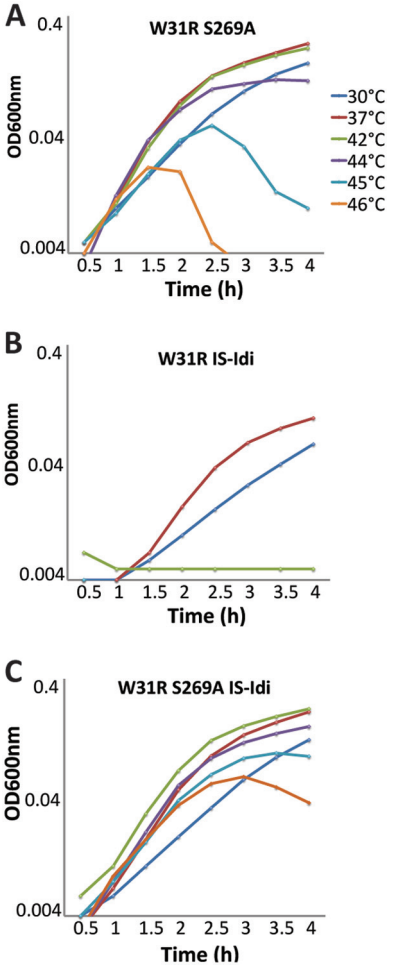

FIG 5 IspH^{S269A} and IS-Idi suppress UppS^{W31R} at different temperatures. Cells were grown in LB at 30°C, 37°C, 42°C, 44°C, 45°C, and 46°C. Growth curves were performed in duplicate, and the data shown are from independent experiments. (A) SKMG198 (UppS^{W31R} IspH^{S269A}). (B) WJM32 (UppS^{W31R} IS-Idi). (C) WJM33 (UppS^{W31R} IspH^{S269A} IS-Idi). W31R, UppS^{W31R}; S269A, IspH^{S269A}.

a strain that could grow at temperatures up to 46°C, though at 45°C and 46°C the cultures reached stationary phase at a lower optical density (Fig. 5C). (Note that our MG1655 strain did not grow above 46°C, meaning that the two suppressors restored growth to this strain's upper limit.) In short, IspH^{S269A} by itself suppressed *uppS31* more efficiently than did the lack of Idi, but combining the two conditions enabled cells to grow at high temperatures.

Increasing intracellular levels of IPP restores cell shape. Because increasing the production of Und-P restored shape to cells harboring the *uppS31* allele (Fig. 3), we tested if increasing the substrates supplied to UppS^{W31R} would also restore cell shape. UppS condenses FPP and IPP to form Und-PP. To increase the levels of FPP and IPP, we introduced the mevalonate (MEV)-dependent isoprenoid pathway from *Saccharomyces cerevisiae* (34) into *E. coli* MG1655 *uppS31 ispH269*. Adding mevalonate to cells expressing the MEV pathway induces production of IPP, and doing so reversed the shape defects of cells carrying *uppS31 ispH269* at 42°C (Fig. 6A and B) while having no effect on the growth rate of these cells (see Fig. S1 in the supplemental material). The cells were ~23% shorter and ~25% thinner than cells without mevalonate (Table 4). These results suggest that increasing the amount of substrate supplied to UppS^{W31R} increases the level of Und-P, promoting PG synthesis.

The Rcs stress response is induced in cells with *uppS31*. Small changes to PG structure activate the Rcs stress response pathway (46–48). Therefore, if *uppS31* affects

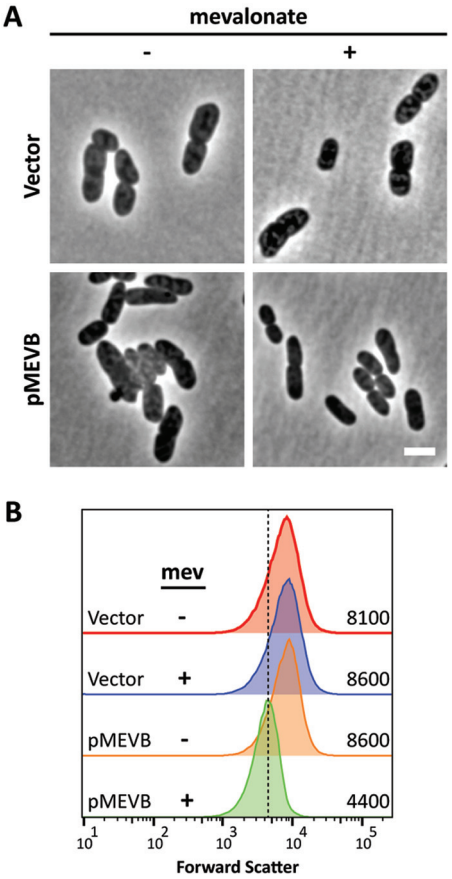

FIG 6 Increased levels of IPP restore cell shape to MG1655 *uppS31 ispH269* (SKMG198) (A) Cells were grown at 42°C in LB to an OD_{600} of 0.4 to 0.5 with (+) or without (−) 2.5 mM mevalonate and photographed by phase-contrast microscopy. The scale bar represents 3 μm. (B) Histograms of the forward-scatter area of 100,000 live cells, as shown in panel A. The mean of the forward-scatter area is reported in arbitrary units to the right of each curve, and the vertical dashed line represents the mean forward scatter of the parent. Vector, pBBR1MC-3; pMEVB, pMEVB.

PG synthesis by decreasing Und-P availability, the presence of *uppS31* may also trigger the Rcs response. We monitored Rcs induction by placing *sfgfp* expression under the control of the Rcs-specific *rprA* promoter. When cells were incubated at 42°C, the Rcs response was induced ~3× more in CS109 *uppS31* than in CS109 *uppS*$^+$ (Fig. 7A and B). Surprisingly, even at 30°C, the Rcs response was induced in CS109 *uppS31* (Fig. 7B). Thus, *uppS31* induces the Rcs response in CS109, suggesting that the mutated enzyme is less efficient even at the permissive temperature.

The W31R replacement severely decreases UppS activity *in vitro*. To assess the effect of the *uppS31* mutation on the production of Und-PP, we monitored the activity of purified UppS$^+$ and UppS^{W31R} by using a fluorescent analogue of FPP,

TABLE 4 Size of *E. coli* MG1655 *uppS31 ispH269* with or without excess IPP

Plasmid	Mevalonate (2.5 mM)	No. of cells at 42°C	Cell size (mean ± SD) (μm)	
			Length	Width
Vector	−	218	4.15 ± 1.22	1.89 ± 0.25
	+	204	4.23 ± 1.27	2.01 ± 0.29
pMevB[a]	−	195	4.09 ± 1.13	1.86 ± 0.28
	+	258	3.15 ± 0.89	1.41 ± 0.19

[a]Plasmid pMEVB was transformed into MG1655 *uppS31 ispH269* to express the enzymes that synthesize IPP from mevalonate.

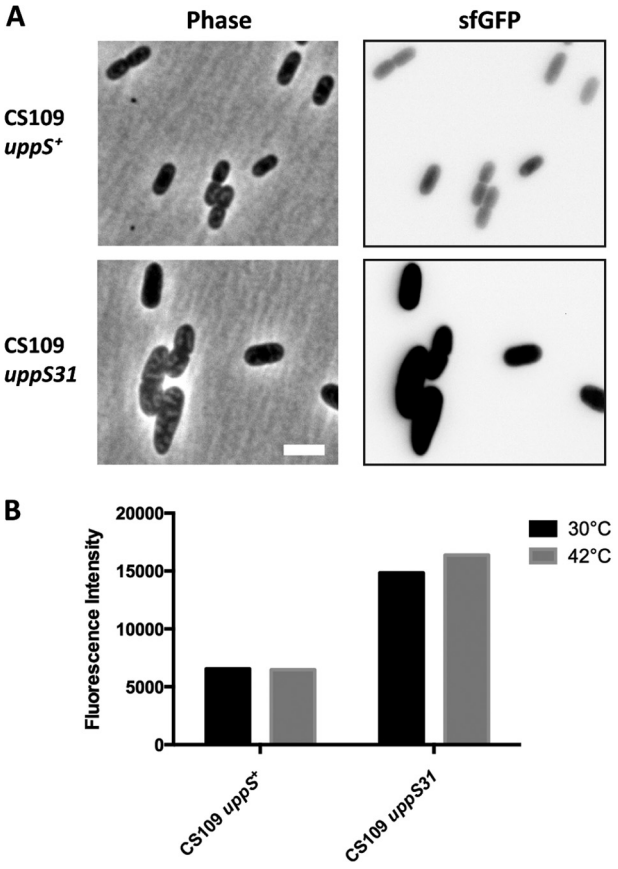

FIG 7 The Rcs stress response is induced when *uppS31* is present. (A) Induction of the Rcs response was monitored by measuring sfGFP from the *rprA* reporter plasmid pDKR1. Cells were grown at 42°C in LB to an OD_{600} of 0.3 to 0.5 and photographed by phase-contrast and fluorescence microscopy. The scale bar represents 3 μm. (B) Cells were grown at 30°C or 42°C in LB. Mean fluorescence intensity is reported in arbitrary units. Strains were CS109 *uppS*$^+$ (SKCS156/pDKR1) and CS109 *uppS31* (CS109/pDKR1).

2-nitrileanilinogeranyl diphosphate (2CNA-GPP) (Fig. 8A) (49). The fluorescence of this compound increases when UppS catalyzes chain elongation (49). UppS$^+$ and UppS^{W31R} activities were tested under steady-state conditions at temperatures ranging from 25°C to 60°C. Compared to the activity of UppS$^+$, the rate of increase in fluorescence with UppS^{W31R} was severely decreased at all temperatures (Fig. 8B). To ensure that the difference in activity was consistent with the amount of product formed, steady-state reactions with mixtures containing 10 μM 2CNA-GPP and 100 nM enzyme were performed for 1 h at 23°C and 42°C and then quenched by adding 1-propanol. Product formation was analyzed by reverse-phase high-performance liquid chromatography (HPLC) (Fig. 8C, 100 nM graphs). UppS$^+$ incorporated 8 to 10 isoprene units into the fluorescent product at 23°C, and at 42°C, most of the product had incorporated 10 isoprene units. However, UppS^{W31R} produced products which had incorporated only 7 or 8 isoprenes, and very little substrate was consumed. Because UppS^{W31R} synthesized much less product than did UppS$^+$, we suspected that UppS^{W31R} had a lower enzyme activity. If so, longer products should accumulate if the reaction time or enzyme concentration was increased. Non-steady-state reactions were prepared with increased concentrations of UppS (1.25 μM UppS^{W31R} and 3.13 μM UppS$^+$), and the products were analyzed by HPLC (Fig. 8C, $>$1 μM UppS). The same smaller products were formed by UppS^{W31R} under these conditions, and the substrate was consumed nearly completely. UppS$^+$ at both 23°C and 42°C gave products identical to those of the 42°C reaction when 100 nM UppS$^+$ was used. Interestingly, UppS^{W31R} activity was not drastically affected by

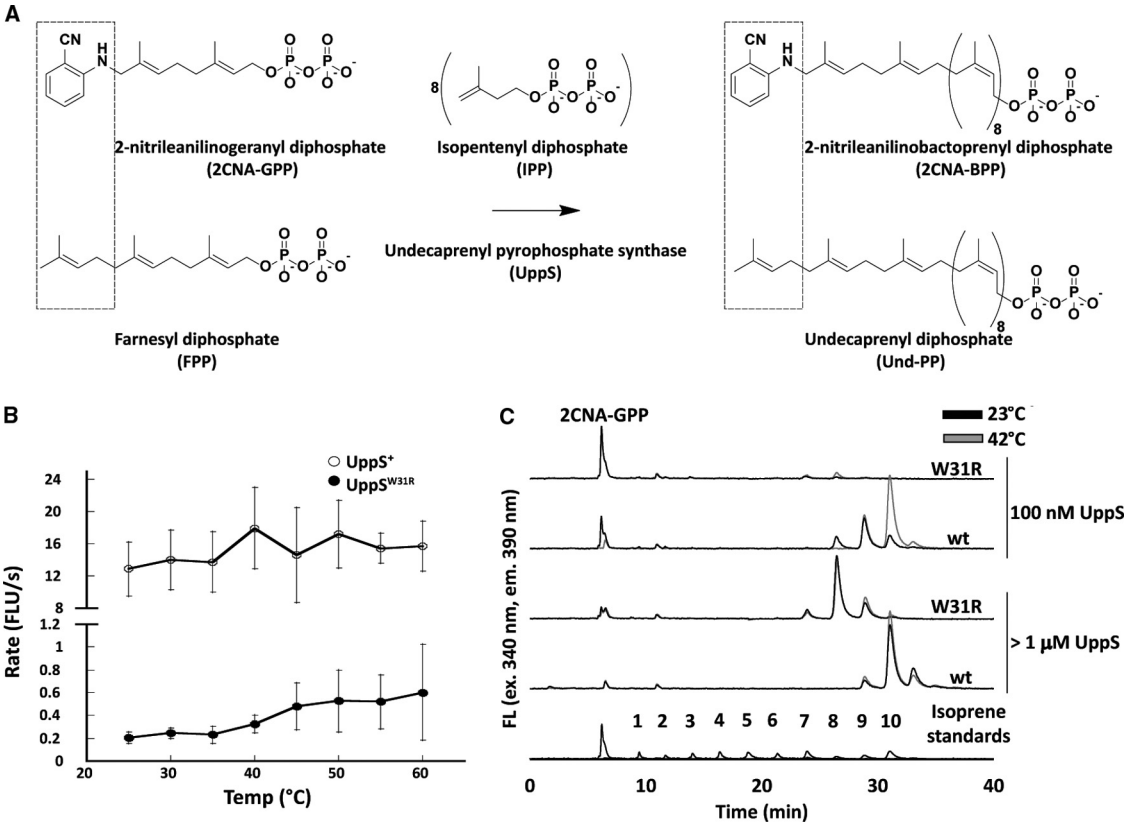

FIG 8 UppS^{W31R} is less active than UppS at all temperatures. (A) Schematic of fluorescent analogue of FPP. The top schematic is our UppS system *in vitro*, and the bottom schematic is what occurs naturally *in vivo*. In the top of the left box is an FPP analog with 2CNA in place of one isoprene unit. The middle shows the reaction of UppS adding 8 additional IPPs to FPP or 2CNA-GPP. The right shows products from the reactions. (B) Reaction mixtures were prepared in a 96-well plate format with 10 μM 2CNA-GPP, 250 μM IPP, and 100 nM UppS cloned from UppS^{+} or UppS^{W31R}. Fluorescence increase over time was monitored at the given temperatures, and the rate of fluorescence increase was plotted. Points represent the average from two different preparations of protein repeated for a minimum of three times, and error bars represent one standard of deviation from the average. Note that the *y* axis is broken to allow visualization of the much slower reaction with UppS^{W31R}. (C) UppS^{+} or UppS^{W31R} in a final volume of 200 μl with 10 μM 2CNA-GPP and 250 μM IPP was incubated at either 23°C or 42°C for 1 h, and the reactions were quenched by adding 50 μl of *n*-propanol. The reaction products were analyzed by HPLC. UppS^{+} and UppS^{W31R} were used at either 100 nM or greater than 1 μM. Isoprene standards were prepared by using *Bacteroides fragilis* UppS in the presence of octyl-thio-glucoside, *n*-dodecyl-β-D-maltoside, and Tween 20. Standards shown are from three separate separations with each detergent, and peak intensity is normalized for the largest product peak in each mixture. The numbers of isoprene units in each peak were previously confirmed by electrospray ionization-mass spectrometry (ESI-MS). FLU, fluorescent light units.

temperature (Fig. 8C). Overall, compared to UppS^{+}, UppS^{W31R} produced shorter polyisoprenoid products and did so at a significantly reduced rate.

The W31R replacement alters UppS folding. Because UppS^{W31R} function was severely degraded, we inspected UppS^{W31R} secondary structure. UppS^{+} and UppS^{W31R} were analyzed by circular dichroism (CD) spectroscopy, and the CD signal clearly differed between the two (Fig. 9), though the relative levels of α-helix to β-sheet were similar (82% α-helix, 1% β-sheet). The data are consistent with a decrease in overall organized secondary structure in UppS^{W31R} compared to the known X-ray crystal structure of *E. coli* UppS (PDB 1X07). This structural change occurred even at low temperature, further suggesting that the mutated enzyme was intrinsically less efficient instead of becoming unfolded at higher temperatures.

DISCUSSION

The *E. coli* K-12 strain CS109 behaves quite differently from the well-known laboratory strain MG1655 in several ways. For example, unlike MG1655, selected CS109 mutants are highly misshapen, do not spiral under certain conditions, and induce the Rcs stress response (50). Also, the cells are highly sensitive to the loss of penicillin-

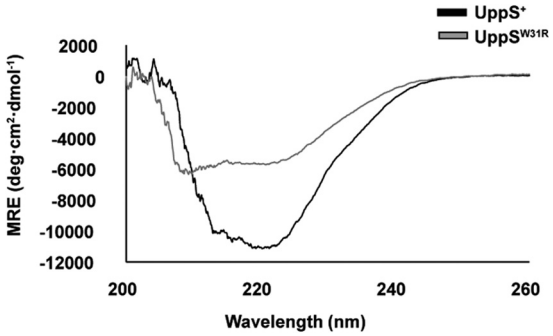

FIG 9 UppS^{W31R} structure is altered relative to UppS^{+}. Circular dichroism spectra were measured at 25°C on 50 μM samples of UppS^{+} and UppS^{W31R}. Both spectra revealed a largely α-helical content of their proteins, but the total organized structure was decreased in UppS^{W31R}. MRE, mean residue ellipticity.

binding protein 1b (PBP1b) (M. Jorgenson, W. MacCain, S. Kannan, B. Meberg, and K. Young, unpublished data), and spheroplasts made from these cells cannot recover their wild-type shapes (D. Ranjit and K. Young, unpublished data). Here, we find that the *uppS* gene of CS109 is mutated so that it expresses a tryptophan-to-arginine missense protein (UppS^{W31R}), and this enzymatically deficient variant supplies too little Und-P to maintain growth or morphology under several conditions. However, these defects are substantially suppressed by compensatory mutations that alter enzymes upstream of UppS in the isoprenoid biosynthesis pathway, indicating the existence of a strong selective pressure for maintaining isoprenoid homeostasis. The results highlight a diverse web of phenotypic traits affected by low Und-P levels, and the defective UppS^{W31R} is a promising new tool for characterizing the *in vivo* activities of enzymes that rely on Und-P-linked substrates.

UppS^{W31R} cannot supply sufficient Und-P to support growth at higher temperatures. UppS^{W31R} is enzymatically deficient at all temperatures *in vitro*, and the enzyme is evidently so defective *in vivo* that it cannot support normal bacterial development even when cells are growing slowly at 30°C. Thus, the temperature-sensitive phenotype is not caused by the denaturation of UppS^{W31R} at higher temperatures; instead, it seems the enzyme simply cannot meet the increased demand for Und-P(P) in cells forced to grow at accelerated rates. A clue for why this occurs is that the tryptophan at position 31 is located in a conserved region that binds FPP, one of two essential substrates for synthesizing Und-PP (51). A known variant at this site, W31F, increases the K_m of UppS for FPP but does not change the k_{cat} or K_m values for IPP, the second essential substrate (52). Thus, UppS^{W31F} requires a higher concentration of FPP to produce Und-PP at the same rate as the wild-type enzyme. Other substitutions at this site may have similar effects. Consistent with this viewpoint is that supplying more FPP to UppS^{W31F} increases the synthesis of Und-PP *in vitro* (52). If this same behavior occurs *in vivo*, supplying more FPP to UppS^{W31R} should allow the mutant to produce more Und-PP, thus reversing the phenotypic defects of *E. coli* CS109. We obtained this predicted result by artificially increasing these *in vivo* substrates, leading us to conclude that UppS^{W31R} synthesizes Und-P(P) at a reduced level *in vivo*, thereby slowing PG synthesis and producing growth and shape defects.

Evolution of *uppS31* and its suppressors. If UppS^{W31R} is enzymatically defective and highly deleterious, how and why did this variant arise? Although *E. coli* accumulates mutations during laboratory growth and storage (53–55), we have been unable to concoct an obvious explanation for why cells containing *uppS31* would appear and survive long enough to accumulate the suppressors present in *E. coli* CS109. It is possible that the *ispH* or *idi* mutations appeared first and increased the production of isoprenoid intermediates, so that *uppS31* arose and reduced the amount of Und-P to nondeleterious levels. However, at the moment, the order of appearance can only be a matter of speculation. Nevertheless, and regardless of its origin, the *uppS31* allele by

itself strongly selects for compensatory mutations, and it is reasonable to surmise that the *ispH269* mutation and the IS*1* insertion upstream of *idi* arose to suppress the unfavorable effects of UppS^{W31R}. Although either *ispH269* or IS*1-idi* partially reverses the effects of *uppS31*, the presence of both alleles is better, consistent with the idea that these secondary mutations increase the amount of Und-P being produced, though not to wild-type levels.

How might IspH^{S269A} reverse the effects of UppS^{W31R}? IspH synthesizes DMAPP and IPP from HMBPP. These products are then combined to make FPP, which is extended by UppS to create Und-PP. IspH residue S269 is located in the cleft where HMBPP binds (56), but no known mutations alter this residue, so it is not clear how substitutions at this site affect the enzymatic activity of IspH. However, if IspH^{S269A} were to make less DMAPP and IPP, the growth and morphological phenotypes observed in cells containing UppS^{W31R} should become worse instead of returning to normal. Also, if IspH^{S269A} were a less active enzyme, the decrease in DMAPP and IPP levels would stress other pathways that rely on these substrates, thus making an already poor situation worse. Therefore, it seems most likely that IspH^{S269A} synthesizes more DMAPP and IPP and funnels these substrates into the Und-P synthesis pathway.

As noted above, UppS^{W31F} has a higher K_m for FPP (52), and by analogy and from evidence presented here, we predict that UppS^{W31R} shares this characteristic. In fact, the semilethal effects of UppS^{W31R} were overcome by increasing the supply of FPP. If IspH^{S269A} makes more substrate that is converted into FPP, this would allow UppS^{W31R} to synthesize more Und-PP. As noted above, increasing the concentrations of IPP and DMAPP allowed cells containing UppS^{W31R} to survive with virtually normal morphology, consistent with the prediction that IspH^{S269A} reverses the effect of UppS^{W31R} by making more of these precursors. In short, the weight of evidence favors the idea that IspH^{S269A} increases the amounts of IPP and DMAPP, thus increasing the supply of FPP, which in turn allows UppS^{W31R} to produce sufficient Und-P to reverse phenotypes triggered by a reduced pool of this lipid carrier.

How might interrupting the expression of *idi* reverse the effects of UppS^{W31R}? In *E. coli*, IspH synthesizes DMAPP and IPP in a ratio of 1:5 or 1:6, after which Idi adjusts this ratio to 7:3 (57). Idi is not essential in organisms that utilize the MEP pathway because DMAPP and IPP are both present (58), but the enzyme is essential in organisms that use only the mevalonate pathway, because this route synthesizes IPP without producing DMAPP (1). The fact that Idi continues to be produced in organisms where it is not essential suggests that there are (unknown) circumstances in which the DMAPP-to-IPP ratio needs to be adjusted. In any event, removing Idi partially suppresses the physiological defects in *E. coli* cells containing UppS^{W31R}, representing the first phenotype to be associated with the loss of *idi*.

In the absence of Idi, the DMAPP-to-IPP ratio decreases from 7:3 to become 1:5 or 1:6 (57). This is counterintuitive in the context of suppressing the effects of UppS^{W31R}, since DMAPP is the initial substrate onto which two IPP molecules are added to create FPP (37). It would seem that more DMAPP, not less, would increase the production of FPP, thus counteracting the high K_m that UppS^{W31R} likely has for this substrate. However, UppS creates Und-PP by adding 8 additional molecules of IPP to FPP, meaning that UppS uses significantly more IPP than DMAPP. However, UppS competes with the IspB enzyme of the quinone pathway for access to a common pool of IPP and FPP (59, 60). Thus, the absence of Idi may increase the pool of IPP to such a degree that UppS^{W31R} can compete more effectively for this substrate. If so, the two suppressors would affect UppS^{W31R} in different ways, helping to explain why both mutations arose in *E. coli* CS109.

UppS^{W31R} activity resembles that of an historical UppS variant. In 1999, when Kato et al. first identified the *uppS* gene (then called *rth*), they also isolated the first temperature-sensitive (ts) variant of UppS (then called UDS) (41). At the nonpermissive temperature, cells containing this variant enlarged and then lysed (41), consistent with our present understanding that a shortage of Und-P inhibits PG synthesis. Unfortunately, the DNA sequence of this temperature-sensitive gene was not determined, and

the mutant itself seems to have been lost and is no longer available for study. However, Kato et al. did measure the levels of ubiquinone and polyprenyl compounds present in their strains. At the nonpermissive temperature (42°C), the mutant produced much smaller amounts of Und-P than did wild-type cells (41). Importantly, the ts mutant made less Und-P even when cells were grown at the permissive temperature (30°C), and there was a corresponding increase in the amounts of ubiquinone and related compounds (41). Looking back, this equilibration can be explained because we now know that the Und-P and quinone biosynthesis pathways both compete for FPP and IPP (59). Thus, when a defective Und-P pathway uses less FPP, more FPP can be diverted to the quinone pathway. The fact that the UppS^{ts} mutant of Kato et al. produced less Und-P even when grown at 30°C strongly implies that this enzyme was less active at all temperatures, suggesting that the Kato UppS^{ts} variant, like UppS^{W31R}, could not supply enough Und-P to meet the increased demand for PG at the higher temperature.

UppS^{W31R} as a tool for probing the *in vivo* activity of Und-P-dependent enzymes. Because cells containing UppS^{W31R} produce less Und-P, these may be used as "indicator strains" to investigate the biochemical and regulatory interactions among pathways that compete for Und-P-linked substrates and other isoprenoids. Und-P is an essential lipid carrier in numerous pathways that transfer carbohydrates and glycans across the cytoplasmic membrane (5), and circumstances that decrease the amount of Und-P cause bacteria to grow slowly, exhibit aberrant morphologies, and lyse (42, 43). Therefore, by using cells carrying UppS^{W31R} and containing a limited amount of Und-P, *in vivo* competition among different Und-P-dependent pathways can be investigated by using overt cell wall-related phenotypes as a physiological readout.

Summary. For 30 years, scientists have probed the structure, activity, and kinetics of undecaprenyl pyrophosphate synthase, as exemplified by the UppS enzyme of *E. coli* (27, 41, 61). However, less effort has been invested in understanding how bacterial physiology responds to alterations in UppS and its substrates or products, or about how interactions among these compounds and pathways affect bacterial growth or behavior. Here, we describe experiments conducted in a noncanonical strain of *E. coli* that further illuminate our understanding of the importance of the isoprenoid Und-P, as well as create a new tool for studying Und-P-related reactions *in vivo*.

MATERIALS AND METHODS

Bacterial strains, plasmids, and media. The bacterial strains, plasmids, and primers used are listed in Tables S1 to S3 in the supplemental material. Bacteria were grown in LB broth (0.5% yeast extract, 1% tryptone, 1% NaCl). Where required, ampicillin (100 $\mu g \cdot ml^{-1}$) or kanamycin (50 $\mu g \cdot ml^{-1}$) was added to select for plasmid maintenance. Cells were grown in baffled flasks or in a Bioscreen C (Automated Microbiology Growth analysis systems). When appropriate, the levels of intracellular IPP were manipulated by adding 2.5 mM DL-mevalonate to the growth medium (62). The Rcs system reporter plasmid pDKR1 (63) expresses superfolder green fluorescent protein (sfGFP) under the control of the Rcs-specific promoter P_{rprA} (64, 65).

Strain construction. To move the wild-type or mutant versions of *uppS* and *ispH* to and from MG1655 or CS109, we used λ-Red recombination to insert a kanamycin resistance cassette in either *btuF* or *thrC*, respectively (66). Following confirmation of kanamycin insertion by diagnostic PCR, the region corresponding to *uppS* or *ispH* was moved by phage P1 cotransduction, followed by PCR confirmation. The IS*1* element upstream of *idi* was removed from CS109 by inserting a kanamycin resistance cassette upstream of the *uacT* gene in MG1655, using λ-Red recombination (66). This gene and the wild-type version of *idi* were cotransduced into CS109. All genetic manipulations were verified by PCR.

Plasmid construction. Plasmids for rescuing CS109 shape defects at 42°C were derivatives of pDSW204 and were constructed as follows. pUppS^{W31R} (P_{204}::*uppS31*) was constructed by amplifying *uppS* from CS109 with primers P21 and P22. The PCR product was cut with EcoRI and HindIII and ligated into the same sites of pDSW204 (67). Plasmids for UppS purification were derivatives of pET24b. pWJM3 (P_{T7}::*uppS*) and pWJM4 (P_{T7}::*uppS31*) were constructed by amplifying *uppS* from either MG1655 or CS109 with primers uppS5′pET24b and uppS3′RCpET24b. The 774-bp PCR product was cut with NdeI and XhoI and ligated into the same sites of pET24b. All constructs were verified by DNA sequencing at the University of Arkansas for Medical Sciences (UAMS) DNA Sequencing Core Facility.

Genomic sequencing and identification of transposition events. The Qiagen genomic DNA buffer set (catalog no. 19060) and Genomic-tip 500/G columns (catalog no. 10262) were used to isolate genomic DNA for whole-genome sequencing. The manufacturer's protocol was followed, with modifications. Libraries were generated with 100 ng of the genomic DNA (gDNA), and the DNA samples were processed using Illumina's Nextera XT library prep kit. Briefly, samples were enzymatically fragmented, and Illumina adapters were simultaneously attached. Nextera indices were then incorporated by limited PCR. The

resulting libraries were purified using AMPure XP magnetic beads (Beckman Coulter), as described in the Nextera XT protocol. Quantification was performed using a Life Technologies Qubit BR assay, and fragment sizing was performed using an Agilent TapeStation 2200 D1000 tape. Libraries were adjusted to 2 μM and sequenced on an Illumina MiSeq platform, using 2 $\times$ 250 V2 chemistry. Sequencing readouts were mapped to the reference genome of *E. coli* MG1655 (RefSeq accession number NC_000913), by using Bowtie2 (68), with the local alignment option. Bam files were converted to Sam files using SAMtools (69). To identify flanking genomic regions, the first and last 50 to 75 bases of each insertion element were identified and extracted, using regular expressions with Galaxy's Select tool. These tools are part of the next-generation sequencing (NGS) collection at https://usegalaxy.org/.

Flow cytometry. Live cells were prepared for flow cytometry and analyzed as described previously (42). Overnight cultures were grown in LB medium at 30°C and were diluted into the same medium at a starting optical density at 600 nm (OD_{600}) of 0.003. These cells were grown to an OD_{600} of ~0.3 to 0.6, at which point cells from 1 ml of this culture were pelleted by centrifugation and resuspended in 1 ml of filtered phosphate-buffered saline (PBS; 137 mM NaCl, 3 mM KCl, 9 mM NaH_2PO_4, and 2 mM KH_2PO_4 [pH 7.4]). Cells were washed twice in PBS, after which cells were diluted 1:10 in PBS to an OD_{600} of ~0.05, and 100,000 cells were analyzed by flow cytometry. Cell size was measured by using the forward-scatter detector mode of a BD LSRFortessa flow cytometer, housed in the UAMS Flow Cytometry Core Facility. Flow data were analyzed with FlowJo version 10.1 software.

Microscopy. Overnight cultures were grown in LB medium at 30°C and were diluted into the same medium at a starting OD_{600} of 0.003. These cells were grown to an OD_{600} of ~0.3 to 0.6, and 5 μl of culture was spotted onto a 1% agarose-covered slide. The morphology of each strain was visualized by phase-contrast microscopy by using an Olympus BX60 microscope fitted with a 100$\times$ oil objective (1.3 numerical aperture [NA] PH3). The fluorescence signal of sfGFP was detected with an enhanced GFP filter set (495 nm excitation and 519 nm emission wavelengths). Cell lengths were measured with cellSens Dimensions software, version 1.6 (Olympus). Images were processed by using ImageJ or Adobe Photoshop software to adjust brightness and contrast (70). Images were cropped and assembled in Adobe Illustrator.

UppS activity assays using 2CNA-GPP. *uppS* genes were expressed, protein was isolated by nickel-nitrilotriacetic acid (Ni-NTA) affinity chromatography, and clones containing the W31R mutation were transformed into *E. coli* C41 and expressed as previously described (71, 72). 2CNA-GPP was prepared as previously described (49). Reaction mixtures contained 25 mM Bicine (pH 8.5), 0.5 mM $MgCl_2$, 5 mM KCl, 0.14% Tween 20, 10 μM 2CNA-GPP, and 100 nM UppS. The reactions were carried out in a 96-well plate format and were initiated by adding 10 μl of IPP to give a final concentration of 250 μM in a final reaction volume of 200 μl. The reaction rates were recorded every 10 to 20 s over 10 to 20 min by monitoring fluorescence excitation at 340 nm and emission at 390 nm by using a Molecular Devices M5 plate reader. For each protein, the assay was performed at least three times, and 2 to 3 different protein preparations were assayed in each experiment. Protein concentrations were determined by measuring the UV absorbance at 280 nm, using the following extinction coefficients: 39,500 $cm^{-1} \cdot M^{-1}$ ($UppS^{+}$) and 33,810 $cm^{-1} \cdot M^{-1}$ ($UppS^{W31R}$). The initial reaction rates based on the increase in fluorescence per unit time were determined for each reaction.

HPLC analysis of UppS reaction products. Reaction mixtures were prepared as described in the UppS activity assay described above but with 500 μM IPP, and they were incubated at 23 or 42°C. After 1 h, the reactions were quenched by adding 50 μl of 1-propanol. Identical reaction mixtures were prepared with 1.25 μM $UppS^{W31R}$ or 3.13 μM $UppS^{+}$, and quenched after 1 h. The reaction products were analyzed by reverse-phase HPLC (RP-HPLC) using fluorescence detection (excitation 340 nm, emission 390 nm), and a C_{18} 4.6 by 150-mm 5-μm column (Agilent). For separation, a gradient was applied as previously described (49), beginning with 15% 1-propanol plus 85% 100 mM ammonium bicarbonate that was raised to 95% over 37 min.

Preparation of the isoprene ladder. The isoprene ladder was prepared from three different reactions with mixtures containing different surfactants, all other components being identical to the reaction as described above. Isoprene additions 1 to 6 were collected from *Bacteroides fragilis* UppS reactions with mixtures containing 10% octylthioglucoside rather than Tween 20. Isoprene additions 7 and 8 were from *B. fragilis* UppS reactions with mixtures containing 1% *n*-dodecyl-β-D-maltoside. Isoprene additions 9 and 10 were from *B. fragilis* UppS reactions with mixtures containing 0.14% Tween 20. *B. fragilis* UppS was used because its activity is readily controlled by varying the surfactant (49).

CD spectroscopy. $UppS^{+}$ and $UppS^{W31R}$ proteins were prepared at a concentration of 50 μM in 50 mM Tris-HCl (pH 8.0) and 200 mM NaCl. CD spectra were collected from 200 to 260 nm at 25°C on a Jasco 1500 CD spectrometer. Under these buffer conditions (lacking surfactant), both the UppS and $UppS^{W31R}$ proteins began precipitating at temperatures of 45°C and above. Data (ellipticity in millidegrees) were transformed to molar residue ellipticity (degrees $\cdot$ $cm^2 \cdot dmol^{-1}$), based on 260 amino acids in the final protein and a 50 μM concentration. Analysis of α-helical and β-sheet contents was performed on K2D2 (73).

SUPPLEMENTAL MATERIAL

Supplemental material for this article may be found at https://doi.org/10.1128/JB.00255-18.

SUPPLEMENTAL FILE 1, PDF file, 0.2 MB.

ACKNOWLEDGMENTS

We thank Michael E. Kovach for plasmid pBBR1MCS-3. We thank Laura Anne Darley for technical assistance. We also thank Andrea Harris of the UAMS Flow Cytometry Core

Facility for help with flow cytometry and analysis and Allen Gies of the UAMS DNA Sequencing Core Facility for help with whole-genome and DNA sequencing. We thank Irina Nesmelova and Diana Joy for help with CD measurements. We also thank Amanda Reid for preparation of 2CNA-GPP and IPP.

The research reported in this publication was supported by the following awards from the Charlotte Research Scholars (JMT) and the U.S. National Institutes of Health, National Institute of General Medical Sciences: R01-GM061019 (to K.D.Y.), R01-GM123251 (to J.M.T.), and R15-GM114773 (to J.M.T.).

REFERENCES

1. Pérez-Gil J, Rodriguez-Concepcion M. 2013. Metabolic plasticity for isoprenoid biosynthesis in bacteria. Biochem J 452:19–25. https://doi.org/10.1042/BJ20121899.
2. Zhao L, Chang WC, Xiao Y, Liu HW, Liu P. 2013. Methylerythritol phosphate pathway of isoprenoid biosynthesis. Annu Rev Biochem 82:497–530. https://doi.org/10.1146/annurev-biochem-052010-100934.
3. Heuston S, Begley M, Gahan CG, Hill C. 2012. Isoprenoid biosynthesis in bacterial pathogens. Microbiology 158:1389–1401. https://doi.org/10.1099/mic.0.051599-0.
4. Gräwert T, Groll M, Rohdich F, Bacher A, Eisenreich W. 2011. Biochemistry of the non-mevalonate isoprenoid pathway. Cell Mol Life Sci 68:3797–3814. https://doi.org/10.1007/s00018-011-0753-z.
5. Manat G, Roure S, Auger R, Bouhss A, Barreteau H, Mengin-Lecreulx D, Touze T. 2014. Deciphering the metabolism of undecaprenyl-phosphate: the bacterial cell-wall unit carrier at the membrane frontier. Microb Drug Resist 20:199–214. https://doi.org/10.1089/mdr.2014.0035.
6. Cui TZ, Kaino T, Kawamukai M. 2010. A subunit of decaprenyl diphosphate synthase stabilizes octaprenyl diphosphate synthase in *Escherichia coli* by forming a high-molecular weight complex. FEBS Lett 584:652–656. https://doi.org/10.1016/j.febslet.2009.12.029.
7. Harada H, Misawa N. 2009. Novel approaches and achievements in biosynthesis of functional isoprenoids in *Escherichia coli*. Appl Microbiol Biotechnol 84:1021–1031. https://doi.org/10.1007/s00253-009-2166-6.
8. Becker J, Wittmann C. 2016. Systems metabolic engineering of *Escherichia coli* for the heterologous production of high value molecules-a veteran at new shores. Curr Opin Biotechnol 42:178–188. https://doi.org/10.1016/j.copbio.2016.05.004.
9. Li Y, Wang G. 2016. Strategies of isoprenoids production in engineered bacteria. J Appl Microbiol 121:932–940. https://doi.org/10.1111/jam.13237.
10. Sprenger GA, Schorken U, Wiegert T, Grolle S, de Graaf AA, Taylor SV, Begley TP, Bringer-Meyer S, Sahm H. 1997. Identification of a thiamin-dependent synthase in *Escherichia coli* required for the formation of the 1-deoxy-D-xylulose 5-phosphate precursor to isoprenoids, thiamin, and pyridoxol. Proc Natl Acad Sci U S A 94:12857–12862.
11. Rohdich F, Hecht S, Gartner K, Adam P, Krieger C, Amslinger S, Arigoni D, Bacher A, Eisenreich W. 2002. Studies on the nonmevalonate terpene biosynthetic pathway: metabolic role of IspH (LytB) protein. Proc Natl Acad Sci U S A 99:1158–1163. https://doi.org/10.1073/pnas.032658999.
12. Fujisaki S, Nishino T, Katsuki H. 1986. Isoprenoid synthesis in *Escherichia coli*. Separation and partial purification of four enzymes involved in the synthesis. J Biochem 99:1327–1337.
13. Tytgat HL, Lebeer S. 2014. The sweet tooth of bacteria: common themes in bacterial glycoconjugates. Microbiol Mol Biol Rev 78:372–417. https://doi.org/10.1128/MMBR.00007-14.
14. Lombard J. 2016. The multiple evolutionary origins of the eukaryotic *N*-glycosylation pathway. Biol Direct 11:36. https://doi.org/10.1186/s13062-016-0137-2.
15. Varki A. 2017. Biological roles of glycans. Glycobiology 27:3–49. https://doi.org/10.1093/glycob/cww086.
16. Higashi Y, Strominger JL, Sweeley CC. 1967. Structure of a lipid intermediate in cell wall peptidoglycan synthesis: a derivative of a C55 isoprenoid alcohol. Proc Natl Acad Sci U S A 57:1878–1884. https://doi.org/10.1073/pnas.57.6.1878.
17. Umbreit JN, Strominger JL. 1972. Isolation of the lipid intermediate in peptidoglycan biosynthesis from *Escherichia coli*. J Bacteriol 112:1306–1309.
18. Watkinson RJ, Hussey H, Baddiley J. 1971. Shared lipid phosphate carrier in the biosynthesis of teichoic acid and peptidoglycan. Nat New Biol 229:57–59. https://doi.org/10.1038/newbio229057a0.
19. Rick PD, Hubbard GL, Kitaoka M, Nagaki H, Kinoshita T, Dowd S, Simplaceanu V, Ho C. 1998. Characterization of the lipid-carrier involved in the synthesis of enterobacterial common antigen (ECA) and identification of a novel phosphoglyceride in a mutant of *Salmonella* Typhimurium defective in ECA synthesis. Glycobiology 8:557–567. https://doi.org/10.1093/glycob/8.6.557.
20. Wright A, Dankert M, Fennessey P, Robbins PW. 1967. Characterization of a polyisoprenoid compound functional in O-antigen biosynthesis. Proc Natl Acad Sci U S A 57:1798–1803.
21. Troy FA, Frerman FE, Heath EC. 1971. The biosynthesis of capsular polysaccharide in *Aerobacter aerogenes*. J Biol Chem 246:118–133.
22. Feldman MF, Wacker M, Hernandez M, Hitchen PG, Marolda CL, Kowarik M, Morris HR, Dell A, Valvano MA, Aebi M. 2005. Engineering N-linked protein glycosylation with diverse O antigen lipopolysaccharide structures in *Escherichia coli*. Proc Natl Acad Sci U S A 102:3016–3021. https://doi.org/10.1073/pnas.0500044102.
23. Guan S, Bastin DA, Verma NK. 1999. Functional analysis of the O antigen glucosylation gene cluster of *Shigella flexneri* bacteriophage SfX. Microbiology 145:1263–1273. https://doi.org/10.1099/13500872-145-5-1263.
24. Schmid J, Sieber V, Rehm B. 2015. Bacterial exopolysaccharides: biosynthesis pathways and engineering strategies. Front Microbiol 6:496. https://doi.org/10.3389/fmicb.2015.00496.
25. Trent MS, Ribeiro AA, Doerrler WT, Lin S, Cotter RJ, Raetz CR. 2001. Accumulation of a polyisoprene-linked amino sugar in polymyxin-resistant *Salmonella* Typhimurium and *Escherichia coli*: structural characterization and transfer to lipid A in the periplasm. J Biol Chem 276:43132–43144. https://doi.org/10.1074/jbc.M106962200.
26. Weissborn AC, Rumley MK, Kennedy EP. 1991. Biosynthesis of membrane-derived oligosaccharides. Membrane-bound glucosyltransferase system from *Escherichia coli* requires polyprenyl phosphate. J Biol Chem 266:8062–8067.
27. Baba T, Muth J, Allen CM. 1985. Photoaffinity labeling of undecaprenyl pyrophosphate synthetase with a farnesyl pyrophosphate analogue. J Biol Chem 260:10467–10473.
28. Brown S, Santa Maria JP, Jr, Walker S. 2013. Wall teichoic acids of Gram-positive bacteria. Annu Rev Microbiol 67:313–336. https://doi.org/10.1146/annurev-micro-092412-155620.
29. Meier-Dieter U, Starman R, Barr K, Mayer H, Rick PD. 1990. Biosynthesis of enterobacterial common antigen in *Escherichia coli*. Biochemical characterization of Tn*10* insertion mutants defective in enterobacterial common antigen synthesis. J Biol Chem 265:13490–13497.
30. Samuel G, Reeves P. 2003. Biosynthesis of O-antigens: genes and pathways involved in nucleotide sugar precursor synthesis and O-antigen assembly. Carbohydr Res 338:2503–2519. https://doi.org/10.1016/j.carres.2003.07.009.
31. Typas A, Banzhaf M, Gross CA, Vollmer W. 2011. From the regulation of peptidoglycan synthesis to bacterial growth and morphology. Nat Rev Microbiol 10:123–136. https://doi.org/10.1038/nrmicro2677.
32. Whitfield C. 2006. Biosynthesis and assembly of capsular polysaccharides in *Escherichia coli*. Annu Rev Biochem 75:39–68. https://doi.org/10.1146/annurev.biochem.75.103004.142545.
33. Sanyal S, Menon AK. 2009. Flipping lipids: why an' what's the reason for? ACS Chem Biol 4:895–909. https://doi.org/10.1021/cb900163d.
34. Martin VJ, Pitera DJ, Withers ST, Newman JD, Keasling JD. 2003. Engineering a mevalonate pathway in *Escherichia coli* for production of terpenoids. Nat Biotechnol 21:796–802. https://doi.org/10.1038/nbt833.
35. Campbell TL, Brown ED. 2002. Characterization of the depletion of 2-*C*-methyl-D-erythritol-2,4-cyclodiphosphate synthase in *Escherichia coli* and *Bacillus subtilis*. J Bacteriol 184:5609–5618. https://doi.org/10.1128/JB.184.20.5609-5618.2002.
36. Matsumoto Y, Yasukawa J, Ishii M, Hayashi Y, Miyazaki S, Sekimizu K.

2016. A critical role of mevalonate for peptidoglycan synthesis in *Staphylococcus aureus*. Sci Rep 6:22894. https://doi.org/10.1038/srep22894.
37. Fujisaki S, Takahashi I, Hara H, Horiuchi K, Nishino T, Nishimura Y. 2005. Disruption of the structural gene for farnesyl diphosphate synthase in *Escherichia coli*. J Biochem 137:395–400. https://doi.org/10.1093/jb/mvi049.
38. Krute CN, Carroll RK, Rivera FE, Weiss A, Young RM, Shilling A, Botlani M, Varma S, Baker BJ, Shaw LN. 2015. The disruption of prenylation leads to pleiotropic rearrangements in cellular behavior in *Staphylococcus aureus*. Mol Microbiol 95:819–832. https://doi.org/10.1111/mmi.12900.
39. Shiomi D, Niki H. 2011. A mutation of *ispA* that is involved in isoprenoid biogenesis can improve growth of *Escherichia coli* at low temperatures. Microbiol Immunol 55:885–888. https://doi.org/10.1111/j.1348-0421.2011.00391.x.
40. Fujisaki S, Nishino T, Katsuki H, Hara H, Nishimura Y, Hirota Y. 1989. Isolation and characterization of an *Escherichia coli* mutant having temperature-sensitive farnesyl diphosphate synthase. J Bacteriol 171:5654–5658. https://doi.org/10.1128/jb.171.10.5654-5658.1989.
41. Kato J, Fujisaki S, Nakajima K, Nishimura Y, Sato M, Nakano A. 1999. The *Escherichia coli* homologue of yeast RER2, a key enzyme of dolichol synthesis, is essential for carrier lipid formation in bacterial cell wall synthesis. J Bacteriol 181:2733–2738.
42. Jorgenson MA, Kannan S, Laubacher ME, Young KD. 2016. Dead-end intermediates in the enterobacterial common antigen pathway induce morphological defects in *Escherichia coli* by competing for undecaprenyl phosphate. Mol Microbiol 100:1–14. https://doi.org/10.1111/mmi.13284.
43. Jorgenson MA, Young KD. 2016. Interrupting biosynthesis of O antigen or the lipopolysaccharide core produces morphological defects in *Escherichia coli* by sequestering undecaprenyl phosphate. J Bacteriol 198:3070–3079. https://doi.org/10.1128/JB.00550-16.
44. Farha MA, Czarny TL, Myers CL, Worrall LJ, French S, Conrady DG, Wang Y, Oldfield E, Strynadka NC, Brown ED. 2015. Antagonism screen for inhibitors of bacterial cell wall biogenesis uncovers an inhibitor of undecaprenyl diphosphate synthase. Proc Natl Acad Sci U S A 112:11048–11053. https://doi.org/10.1073/pnas.1511751112.
45. Young KD. 2010. Bacterial shape: two-dimensional questions and possibilities. Annu Rev Microbiol 64:223–240. https://doi.org/10.1146/annurev.micro.112408.134102.
46. Evans KL, Kannan S, Li G, de Pedro MA, Young KD. 2013. Eliminating a set of four penicillin binding proteins triggers the Rcs phosphorelay and Cpx stress responses in *Escherichia coli*. J Bacteriol 195:4415–4424. https://doi.org/10.1128/JB.00596-13.
47. Laubacher ME, Ades SE. 2008. The Rcs phosphorelay is a cell envelope stress response activated by peptidoglycan stress and contributes to intrinsic antibiotic resistance. J Bacteriol 190:2065–2074. https://doi.org/10.1128/JB.01740-07.
48. Majdalani N, Gottesman S. 2005. The Rcs phosphorelay: a complex signal transduction system. Annu Rev Microbiol 59:379–405. https://doi.org/10.1146/annurev.micro.59.050405.101230.
49. Troutman JM, Erickson KM, Scott PM, Hazel JM, Martinez CD, Dodbele S. 2015. Tuning the production of variable length, fluorescent polyisoprenoids using surfactant-controlled enzymatic synthesis. Biochemistry 54:2817–2827. https://doi.org/10.1021/acs.biochem.5b00310.
50. Ghosh AS, Melquist AL, Young KD. 2006. Loss of O-antigen increases cell shape abnormalities in penicillin-binding protein mutants of *Escherichia coli*. FEMS Microbiol Lett 263:252–257. https://doi.org/10.1111/j.1574-6968.2006.00429.x.
51. Chang SY, Ko TP, Chen AP, Wang AH, Liang PH. 2004. Substrate binding mode and reaction mechanism of undecaprenyl pyrophosphate synthase deduced from crystallographic studies. Protein Sci 13:971–978. https://doi.org/10.1110/ps.03519904.
52. Chen YH, Chen AP, Chen CT, Wang AH, Liang PH. 2002. Probing the conformational change of *Escherichia coli* undecaprenyl pyrophosphate synthase during catalysis using an inhibitor and tryptophan mutants. J Biol Chem 277:7369–7376. https://doi.org/10.1074/jbc.M110014200.
53. Desroches M, Royer G, Roche D, Mercier-Darty M, Vallenet D, Medigue C, Bastard K, Rodriguez C, Clermont O, Denamur E, Decousser JW. 2018. The odyssey of the ancestral Escherich strain through culture collections: an example of allopatric diversification. mSphere 3:e00553-17. https://doi.org/10.1128/mSphere.00553-17.
54. Freddolino PL, Amini S, Tavazoie S. 2012. Newly identified genetic variations in common *Escherichia coli* MG1655 stock cultures. J Bacteriol 194:303–306. https://doi.org/10.1128/JB.06087-11.
55. Liu B, Eydallin G, Maharjan RP, Feng L, Wang L, Ferenci T. 2017. Natural *Escherichia coli* isolates rapidly acquire genetic changes upon laboratory domestication. Microbiology 163:22–30. https://doi.org/10.1099/mic.0.000405.
56. Gräwert T, Span I, Eisenreich W, Rohdich F, Eppinger J, Bacher A, Groll M. 2010. Probing the reaction mechanism of IspH protein by x-ray structure analysis. Proc Natl Acad Sci U S A 107:1077–1081. https://doi.org/10.1073/pnas.0913045107.
57. Rohdich F, Zepeck F, Adam P, Hecht S, Kaiser J, Laupitz R, Grawert T, Amslinger S, Eisenreich W, Bacher A, Arigoni D. 2003. The deoxyxylulose phosphate pathway of isoprenoid biosynthesis: studies on the mechanisms of the reactions catalyzed by IspG and IspH protein. Proc Natl Acad Sci U S A 100:1586–1591. https://doi.org/10.1073/pnas.0337742100.
58. Hahn FM, Hurlburt AP, Poulter CD. 1999. *Escherichia coli* open reading frame 696 is *idi*, a nonessential gene encoding isopentenyl diphosphate isomerase. J Bacteriol 181:4499–4504.
59. Pan JJ, Kuo TH, Chen YK, Yang LW, Liang PH. 2002. Insight into the activation mechanism of *Escherichia coli* octaprenyl pyrophosphate synthase derived from pre-steady-state kinetic analysis. Biochim Biophys Acta 1594:64–73. https://doi.org/10.1016/S0167-4838(01)00283-7.
60. Lee PC, Salomon C, Mijts B, Schmidt-Dannert C. 2008. Biosynthesis of ubiquinone compounds with conjugated prenyl side chains. Appl Environ Microbiol 74:6908–6917. https://doi.org/10.1128/AEM.01495-08.
61. Pan JJ, Chiou ST, Liang PH. 2000. Product distribution and pre-steady-state kinetic analysis of *Escherichia coli* undecaprenyl pyrophosphate synthase reaction. Biochemistry 39:10936–10942. https://doi.org/10.1021/bi000992l.
62. Campos N, Rodriguez-Concepcion M, Sauret-Gueto S, Gallego F, Lois LM, Boronat A. 2001. *Escherichia coli* engineered to synthesize isopentenyl diphosphate and dimethylallyl diphosphate from mevalonate: a novel system for the genetic analysis of the 2-*C*-methyl-D-erythritol 4-phosphate pathway for isoprenoid biosynthesis. Biochem J 353:59–67. https://doi.org/10.1042/bj3530059.
63. Ranjit DK, Young KD. 2013. The Rcs stress response and accessory envelope proteins are required for *de novo* generation of cell shape in *Escherichia coli*. J Bacteriol 195:2452–2462. https://doi.org/10.1128/JB.00160-13.
64. Dinh T, Bernhardt TG. 2011. Using superfolder green fluorescent protein for periplasmic protein localization studies. J Bacteriol 193:4984–4987. https://doi.org/10.1128/JB.00315-11.
65. Pédelacq JD, Cabantous S, Tran T, Terwilliger TC, Waldo GS. 2006. Engineering and characterization of a superfolder green fluorescent protein. Nat Biotechnol 24:79–88. https://doi.org/10.1038/nbt1172.
66. Datsenko KA, Wanner BL. 2000. One-step inactivation of chromosomal genes in *Escherichia coli* K-12 using PCR products. Proc Natl Acad Sci U S A 97:6640–6645. https://doi.org/10.1073/pnas.120163297.
67. Weiss DS, Chen JC, Ghigo JM, Boyd D, Beckwith J. 1999. Localization of FtsI (PBP3) to the septal ring requires its membrane anchor, the Z ring, FtsA, FtsQ, and FtsL. J Bacteriol 181:508–520.
68. Langmead B, Trapnell C, Pop M, Salzberg SL. 2009. Ultrafast and memory-efficient alignment of short DNA sequences to the human genome. Genome Biol 10:R25. https://doi.org/10.1186/gb-2009-10-3-r25.
69. Li H, Handsaker B, Wysoker A, Fennell T, Ruan J, Homer N, Marth G, Abecasis G, Durbin R, 1000 Genome Project Data Processing Subgroup. 2009. The Sequence Alignment/Map format and SAMtools. Bioinformatics 25:2078–2079. https://doi.org/10.1093/bioinformatics/btp352.
70. Schneider CA, Rasband WS, Eliceiri KW. 2012. NIH Image to ImageJ: 25 years of image analysis. Nat Methods 9:671–675. https://doi.org/10.1038/nmeth.2089.
71. Dodbele S, Martinez CD, Troutman JM. 2014. Species differences in alternative substrate utilization by the antibacterial target undecaprenyl pyrophosphate synthase. Biochemistry 53:5042–5050. https://doi.org/10.1021/bi500545g.
72. Lujan DK, Stanziale JA, Mostafavi AZ, Sharma S, Troutman JM. 2012. Chemoenzymatic synthesis of an isoprenoid phosphate tool for the analysis of complex bacterial oligosaccharide biosynthesis. Carbohydr Res 359:44–53. https://doi.org/10.1016/j.carres.2012.06.014.
73. Louis-Jeune C, Andrade-Navarro MA, Perez-Iratxeta C. 2012. Prediction of protein secondary structure from circular dichroism using theoretically derived spectra. Proteins 80:374–381. https://doi.org/10.1002/prot.23188.